FRONTIERS OF PHYSICS

RESEARCH ARTICLE
Volume 19 / Issue 6 / 63205 / 2024

Multi-conditioned controlled growth of CoBi nanostructures on $SrTiO_3$

Desheng Cai[1,2,*], Yumin Xia[1,2,*], Pengju Li[1,2], Kun Xie[1,2], Yuzhou Liu[1,2], Yitong Gu[1,2], Gan Yu[1,2], Changgan Zeng[1,2,3], Ping Cui[1,3], Shengyong Qin[1,2,3,†]

1 International Center for Quantum Design of Functional Materials (ICQD), University of Science and Technology of China, Hefei 230026, China
2 CAS Key Laboratory of Strongly Coupled Quantum Matter Physics, Department of Physics, University of Science and Technology of China, Hefei 230026, China
3 Hefei National Laboratory, University of Science and Technology of China, Hefei 230088, China
*These authors contributed equally to this work.
Corresponding author. E-mail: †syqin@ustc.edu.cn
Received August 25, 2023; accepted May 4, 2024

ABSTRACT

Cobalt pnictides have been theoretically proposed to be attractive candidates for high-temperature superconductors. Additionally, monolayered CoX (X = As, Sb, Bi) on $SrTiO_3$ systems present a potential new platform for realizing topological superconductors in the two-dimensional limit, due to their nontrivial band topology. To this end, we have successfully fabricated high-quality CoBi nanoislands on $SrTiO_3$ (001) substrates by molecular beam epitaxy followed by an investigation of their atomic structure and electronic properties via in situ scanning tunneling microscopy/spectroscopy. Beyond the previously predicted lattice with $a = b = 3.5$ Å, 2×1 dimer row was observed in this study. Furthermore, our results reveal that the topography of CoBi islands is strongly influenced by various growth conditions, such as substrate temperature, the flux ratio between Co and Bi, and the annealing process. This study paves the way for further explorations of the superconductivity and topological properties of cobalt pnictide systems.

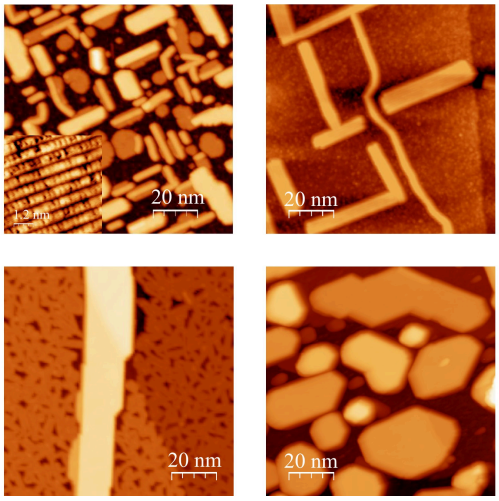

Keywords $CoBi/SrTiO_3$, molecular beam epitaxy, scanning tunneling microscopy, scanning tunneling spectroscopy, nanostructure

1 Introduction

The quest for advanced materials with novel properties has been a focal point in condensed matter physics in recent years. Particularly, the discovery of cuprate [1–3], iron-based [4–7] and nickelate [8–11] high-temperature superconductors has presented new opportunities for exploring new superconducting materials. In addition to exploring new materials, thinning crystalline materials to the two-dimensional (2D) limit offers a versatile playground. One attractive material in this regard is monolayer FeSe, which possesses a simple structure and rich physical properties [12–14]. The monolayer $FeSe/SrTiO_3$ system exhibits a large superconducting gap of up to 20 meV [15], whose transition temperature is characterized around 65 K [16]. Recent studies have shown that the synthesis of 2D materials lacking analogous bulk allotropes exhibit a substantial breadth of physical and chemical properties through the diverse structural options facilitated by substrate-dependent epitaxy

Higher Education Press

https://doi.org/10.1007/s11467-024-1423-6

[17–21]. For instance, the 2D forms of tellurium were theoretically predicted and experimentally confirmed [22, 23], and subsequent study demonstrated that these 2D tellurium harbor exceptional photoresponse behaviors spanning from the UV to the visible regime, coupled with robust time and cycle stability for on/off switching behaviors [24]. These developments have effectively broadened the research region of novel 2D systems.

More recently, theoretical studies have proposed that cobalt pnictides CoX (X = As, Sb, Bi) are appealing new candidate systems of superconductors. These pnictides are predicted to exhibit superconducting properties comparable to FeSe, attributed to their identical valence electrons and similar PbO-type planar crystal phase. PbO-type cobalt pnictides are thermodynamically stable on $SrTiO_3$ substrate through the *ab initio* molecular dynamics simulations although it has no resemblance phase in bulk [25, 26]. More interestingly, $CoX/SrTiO_3$ systems also exhibit a topologically protected one-dimensional edge state due to the strong spin–orbit coupling (SOC) effect, which can invert the band between the conduction band minimum and valence band maximum at the Γ point [26]. The more recent orthorhombic CoSb monolayer has been fabricated on $SrTiO_3$. Furthermore, 14 meV gap around the Fermi level could be observed and vibrating sample magnetometer magnetization drop occurs at 14 K, which shows a signature of superconductivity in CoSb monolayer films on $SrTiO_3$ [27]. Furthermore, the study of the electronic structure of quasi-one-dimensional $CoSb_{1-x}$ strip reports the power-law-like suppression of spectral weight, which obeys a universal temperature scaling, revealing the signature of Tomonaga–Luttinger state [28]. CoBi has the largest electron–phonon coupling strength compared with CoAs and CoSb, which plays an important role in FeSe-based superconductors [29–31], and the strongest SOC strength to induce band inversion. Therefore, probing the growth conditions and electronic structures of $CoBi/SrTiO_3$ is very desirable.

In this work, we successfully obtained 2D CoBi nanoislands on $SrTiO_3$ (001) substrates utilizing molecular beam epitaxy (MBE) and investigated the structure and morphology of CoBi islands using in situ scanning tunneling microscopy (STM). In addition to the obtained lattice constants, $a = b = 3.5$ Å, which is consistent with the theoretical prediction, we also observed a 2×1 dimer row configuration. Furthermore, we found that the topography of CoBi islands is strongly influenced by growth conditions. By meticulously controlling the substrate temperature, flux ratio and annealing process, we were able to fabricate diverse nanostructures, including CoBi nanoislands, nanomeshes, and nanowires. Our approach provides an attractive platform to understand the new types of cobalt pnictides on $SrTiO_3$ (001) substrates and explore the possibility of high-temperature superconductivity and topological properties.

2 Methods

In this study, we utilized MBE to grow CoBi nanoislands on $SrTiO_3$ (001) substrates. Prior to the deposition, 0.7% Nb-doped $SrTiO_3$ substrates were subjected to a high-temperature treatment at 1450 K for 20 minutes to attain a smooth TiO_2-terminated surface. High-purity Co (99.999%) and Bi (99.999%) were thermally evaporated from Knudsen cells, maintaining the pressure below 1×10^{-9} Torr during the MBE growth. The growth of CoBi islands is strongly influenced by the substrate temperature and the flux ratio between Co and Bi. To obtain a high quantity of CoBi islands, we meticulously modulated the substrate temperature and flux ratio. Initially, the Co and Bi cell temperatures were set to 1320 K and 630 K, respectively, with the substrates temperature held at 430 K, facilitating the formation of CoBi islands. While cooling the substrates to 100 K, we increased the Co cell temperature to 1420 K and the Bi cell temperature at 670 K to form nanomesh and further promote island growth. For the growth of nanowires, we increased the substrate temperature to 500 K and set the Co and Bi cell temperatures at 1320 K and 670 K, respectively, to achieve a Bi-rich environment. Additionally, when depositing on substrates at room temperature, we evaporated Co and Bi at 1370 K and 680 K, respectively. To characterize the samples, we employed in situ STM and scanning tunneling spectroscopy (STS) using a Unisoku USM 1500s system. Measurements were conducted at approximately 78 K and 4.2 K, with a base pressure of 2×10^{-10} Torr. STM topographic images were obtained in a constant current mode using chemically etched tungsten tips, while tunneling spectra were acquired using the standard lock-in method with small bias modulations at 0.937 KHz. Image processing was performed with the WSXM program [32].

3 Results and discussion

Figure 1(a) shows a typical STM topographic image of CoBi islands grown on a $SrTiO_3$ substrate at 430 K. The growth of the CoBi islands follows the Stranski–Krastanov mode (i.e., islands start to form after the growth of a CoBi wetting layer), like Pb growth on Si (111) [33, 34], and the sizes of the CoBi islands range from 100 to 300 nm^2. From the line profile in Fig. 1(b), it is noted that the apparent height of the thinnest CoBi islands is approximately 1 nm. In contrast, for thicker islands, STM line profiles consistently reveal layer heights of 0.6 nm. The variation in layer height may be attributed to the formation of a wetting layer between CoBi islands, similar to the Pb islands grown on Si (111) [35]. Additionally, an atomically resolved image of CoBi nanoislands taken at 4.2 K is displayed in Fig. 1(c), revealing periodic stripes and a rectangular lattice. The fast Fourier transform

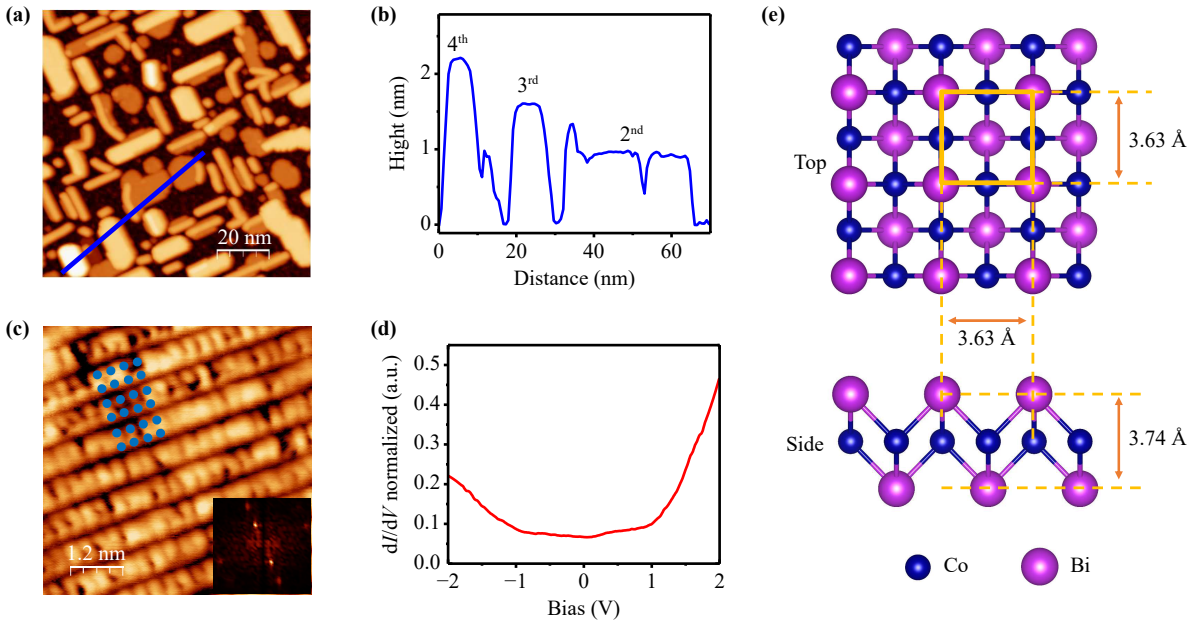

Fig. 1 Epitaxial growth of CoBi on $SrTiO_3$ (001) substrate. **(a)** Topographic image (100 nm × 100 nm, $U = +8$ V, $I =$ 10 pA) of CoBi islands grown on $SrTiO_3$ at 430 K. **(b)** Cross section of the STM image along the line in (a) (blue). **(c)** Atomically resolved topography measured on a CoBi island (6 nm × 6 nm, $U = -0.7$ V, $I = -100$ pA); the inset shows the fast Fourier transform (FFT) of the atomically resolved STM image of CoBi. **(d)** Typical dI/dV tunneling spectrum taken on the CoBi island. **(e)** PbO-type monolayered CoBi. The upper and lower panels show the top and side views, respectively. Reproduced with permission from Ref. [26].

(FFT) pattern corresponding to the sample indicates in-plane lattice constants of $a = b = 3.5$ Å, which is consistent with theoretical predictions ($a = b = 3.647$ Å in free-standing) [26]. Figure 1(e) displays a schematic representation of the structure predicted by the theory [26]. Moreover, the FFT pattern shows additional peaks located at half of the Bragg reciprocal lattice vectors, suggesting the formation of a 2 × 1 superlattice pattern, where the lattice constants are $a = 3.5$ Å and $b = 7.0$ Å. Notably, this phenomenon resembles to the dimer row observed in Si (100) surface [36]. The formation of dimer rows is attributed to the structural transformation of the dangling bonds of neighboring silicon atoms, leading to the formation of Si–Si dimers, at elevated temperatures. Interestingly, the theoretical simulations do not predict the formation of this 2×1 superlattice, thus raising the question of whether this result is due to surface reconstruction or the formation of a new stable structure. Further investigation is necessary to elucidate the underlying mechanisms responsible for this intriguing phenomenon. The electronic properties of the CoBi islands are shown in Fig. 1(d), and the average differential conductance (dI/dV) spectrum taken on the CoBi islands exhibits a typical metallic feature.

In addition, we have discovered other islands that display periodic stripes with a distinct atomic lattice structure, as illustrated in Figs. 2(a) and (b). Careful examination of the high-resolved atomic images reveals that the positions in adjacent stripes are not aligned,

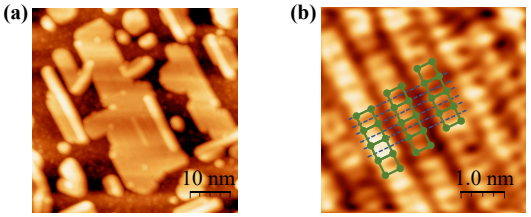

Fig. 2 Mismatched CoBi structure. **(a)** Topographic image (50 nm × 50 nm, $U = +1$ V, $I = 10$ pA) of CoBi islands. **(b)** Atomically resolved topography measured on a CoBi island in (a) (5 nm × 5 nm, $U = +0.235$ V, $I = 110$ pA).

deviating from a typical crystal lattice arrangement. Specifically, there is a horizontal shift of a half lattice constant distance between the adjacent stripes. It is worth noting that in films grown using MBE, defects, dislocations, and lattice distortions often arise. For example, vacancies, which often appear as dark holes in STM topography, are frequently observed in transition metal dichalcogenide materials as a result of the removal of transition metal atoms [37]. Furthermore, dislocations in MBE-grown films can cause lattice distortions and make atoms deviate from their original positions, as is the case for the PbTe epilayers on PbSe (001) [38]. Additionally, lattice strain can induce stripe phase in $La_{0.75}Ca_{0.25}MnO_3/MgO$ systems [39]. In comparison, our finding may be attributed to dislocation or strain-induced effects. Further investigation is required to

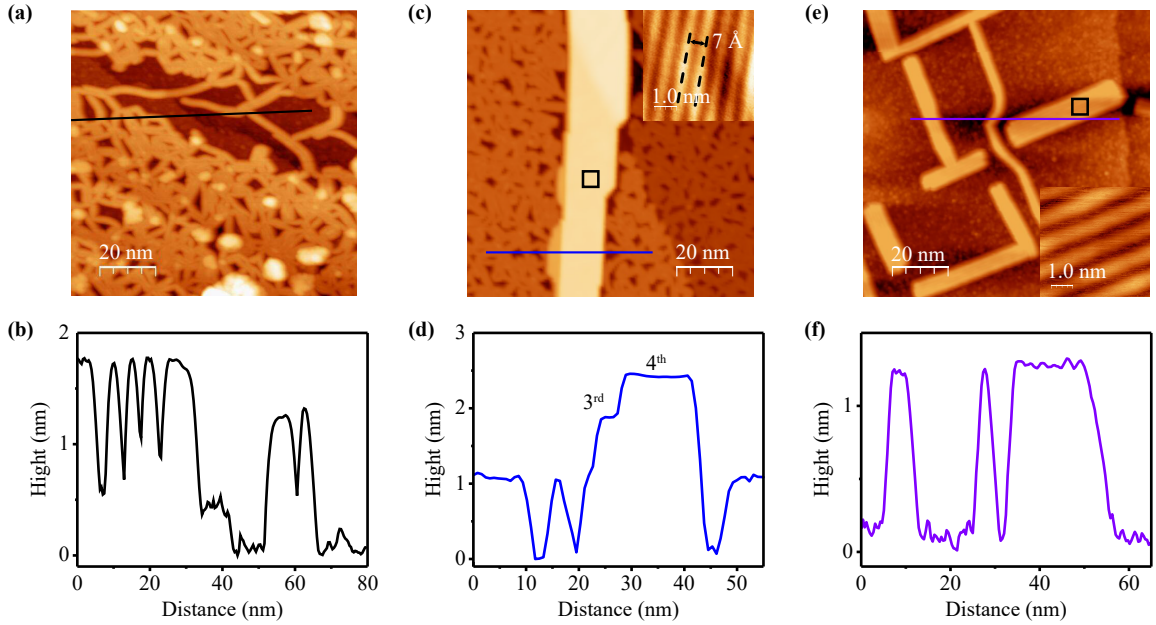

Fig. 3 Impact of varying substrate temperature on CoBi growth. **(a)** Topographic image (100 nm × 100 nm, $U = +2$ V, $I =$ 10 pA) of the CoBi nanomesh grown on $SrTiO_3$ at 100 K after annealing at 393 K for 8 h, Co and Bi cell temperatures at 1420 K and 670 K. **(b)** Cross section of the STM image along the line in (a) (black). **(c)** Topographic image (100 nm × 100 nm, $U = +2$ V, $I = 30$ pA) of CoBi islands grown on $SrTiO_3$ at 100 K after annealing at 393 K for 8 hours, Co and Bi cell temperatures at 1420 K and 670 K; the inset shows the zoomed-in topography of a CoBi islands (5 nm × 5 nm, $U =$ +0.1 V, $I = 200$ pA). **(d)** Cross section of the STM image along the line in (c) (blue). **(e)** Topographic image (100 nm × 100 nm, $U = +1.5$ V, $I = 5$ pA) of CoBi nanowires grown on $SrTiO_3$ at 500 K, Co and Bi cell temperatures at 1320 K and 670 K; the inset shows the zoomed-in topography of a CoBi nanowire showing its striped surface (5 nm × 5 nm, $U = +0.1$ V, $I = 200$ pA). **(f)** Cross section of the STM image along the line in (e) (purple).

understand the underlying mechanisms responsible for this intriguing observation.

The substrate temperature plays a crucial role in MBE growth, affecting both crystalline growth and relaxation processes in heterostructure systems. For example, the modulation of NbN material morphology during MBE growth has been closely examined concerning substrate temperature. At 800 °C, NbN films exhibit a smooth surface with grains having diameters less than 50 nm. Elevating the temperature to 1000 °C results in a surface characterized by parallel striped facets and triangular pyramidal grains. A further increase to 1200 °C yields a surface that is atomically flat on a large scale [40]. In the case of $NbSe_2$, growth at lower temperatures results in randomly branched growth with significantly small feature sizes. As the growth temperature increases, the symmetry improves, and at 600 °C, small triangular islands begin to form [41]. Likewise, in the fabrication of CoSb systems, varying the substrate temperature leads to the formation of different nanostructures such as CoSb nanoislands at 200 °C and CoSb nanomeshes at 380 °C [27]. Thus, precise control of the substrate temperature is essential to achieving the desired film quality and properties in MBE. To further investigate the impact of the growth temperature on the CoBi system, we grew samples over a wide temperature range, resulting in the achievement of two types of CoBi structures at lower growth temperatures. Figure 3(a) presents a topographic image of the CoBi nanomesh grown on $SrTiO_3$ at 100 K after annealing at 393 K for 8 hours. Figure 3(b) provides a depiction of the height of the CoBi nanomesh, which is approximately 1.2 nm surpassing that of the initially mentioned CoBi nanoislands (~1.0 nm). Larger and flatter CoBi islands have been successfully fabricated when the coverage exceeded 0.75 monolayer (ML), as portrayed in the STM image in Fig. 3(c). As depicted in the inset of Fig. 3(c), the CoBi islands show a periodic stripe pattern with a period of 0.7 nm. Additionally, the line profile in Fig. 3(d) indicates that the layer height of CoBi islands is 0.6 nm.

Considering the isostructural and isovalent nature of the FeSe monolayer and CoBi monolayer, we attempted to grow CoBi thin films under Bi-rich conditions and elevated substrate temperatures, referring to the growth conditions of FeSe [15]. At a significantly higher substrate temperature of 500 K, nanowires formed with the coverage of 0.3 ML, as shown in Fig. 3(e). Upon increasing the coverage, clusters begin to occur, indicating that the nanowire coverage limit is ~0.3 ML, akin to CoSb [27]. Interestingly, the nanowires aligned two mutually perpendicular directions differing from the nanomesh shown in Fig. 3(a). Furthermore, all nanowires exhibited periodic stripes along their direction, as shown in Fig. 3(e) inset. As presented in Fig. 3(f),

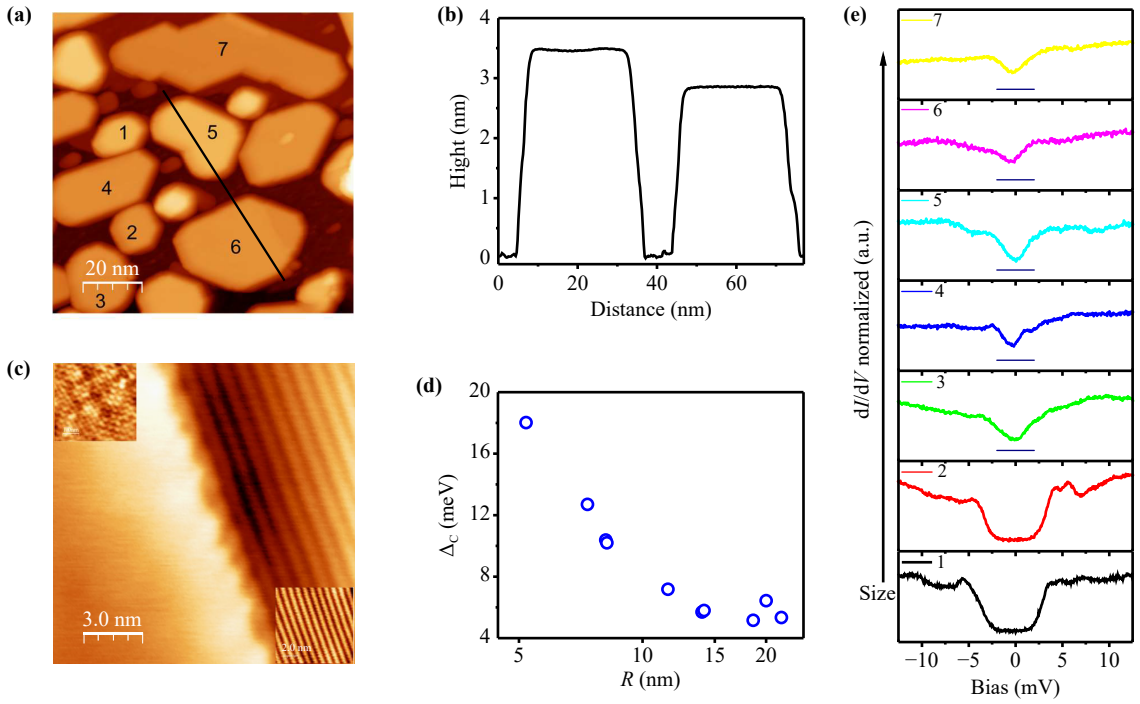

Fig. 4 STM/STS characterization of CoBi islands of different sizes. **(a)** Topographic image (100 nm × 100 nm, $U = +8$ V, $I = 5$ pA) of CoBi islands grown on $SrTiO_3$ at room temperature. **(b)** Cross section of the STM image along the line in (a) (black). **(c)** Zoomed-in topographic image (15 nm × 15 nm, $U = +0.5$ V, $I = 100$ pA) of island number 6. The top inset shows the atomically resolved topography measured in the flattened region in (c) (5 nm × 5 nm, $U = +1$ V, $I = 10$ pA), while the bottom inset shows the zoomed-in topography measured in the striped region in (c) (10 nm × 10 nm, $U = +0.2$ V, $I = 1$ nA). **(d)** Tunneling spectra taken on CoBi islands of different sizes and double logarithmic scale plot of Coulomb gap size and lateral size of CoBi islands. **(e)** Typical tunneling spectra taken on different size CoBi islands.

CoBi nanowires have a height of 1.2 nm, comparable to the height of the nanoislands, yet the stripes on the nanowires exhibited a period of nearly 1.0 nm, which is larger than the period observed on the nanoislands.

To explore the growth of CoBi at moderate temperatures, we grew CoBi islands on $SrTiO_3$ substrate at room temperature, and the STM topography is shown in Fig. 4(a). The majority of these islands are flat, lacking periodic stripes, with a step height approximately 0.6 nm, observed in the line profile in Fig. 4(b). Interestingly, periodic stripes manifest at the corners of a few islands, such as the number 6 island. A zoomed-in image of island number 6, shown in Fig. 4(c), presents the details of the two areas. The period of the stripes, as shown in the bottom inset of Fig. 4(c), is around 0.7 nm, consistent with that observed in CoBi islands. The top inset of Fig. 4(c) displays the atomically resolved topography measured in the flattened region, where a 4.0 Å × 4.7 Å rectangular unit cell can be clearly observed. The lattice structure is similar to that of Bi (110), and the island height corresponds to a bilayer Bi (110). Along the *b*-axis, the lattice constant of these islands is similar to that of Bi (110), though it is narrower along the *a*-axis. Considering that excess Bi remains unevaporated at room temperature, one plausible explanation is the doping of Bi (110) islands with Co, and the characteristics could be further investigated in future research.

Different sizes and ratios of the CoBi islands provide an ideal platform to study their varied electronic properties. Figure 4(e) shows the $\mathrm{d}I/\mathrm{d}V$ tunneling spectra from islands of different sizes, corresponding to those number in Fig. 4(a). The island with the smallest lateral size, denoted as $R = 8$ nm [$R = (\mathrm{area}/\pi)^{1/2}$], exhibits a larger energy gap of approximately 10 meV. Conversely, the largest island ($R = 21$ nm) displays a dip in the density of states at the Fermi energy. Spectra from islands with R values exceeding 11 nm exhibit a dip, whereas those associated with islands smaller than 11 nm manifest characteristics indicative of a Coulomb gap. To clarify the relationship between island size and the $\mathrm{d}I/\mathrm{d}V$ gap, we present Δ_C and R on logarithmic scales in Fig. 4(d). This graphical representation clearly demonstrates a decrease in Δ_C with an increase in the size of the island when R is smaller than 11 nm, consistent with previous observations in the Coulomb gap regime [42]. When R exceeds 14 nm, the Δ_C shows few variations.

4 Conclusions

In conclusion, we have successfully fabricated CoBi islands on $SrTiO_3$ (001) substrates utilizing MBE and

investigated their atomic structure and morphology. The obtained lattice constants are $a = b = 3.5$ Å, which is consistent with theoretical predictions. In addition, we observed an intriguing 2×1 dimer row configuration. Through meticulous manipulation of the growth parameters, specifically the substrate temperature, the flux ratio between Co and Bi, and the annealing process, we achieved the fabrication of various CoBi nanostructures on the $SrTiO_3$ substrates. This achievement allows for a thorough examination of the diverse morphologies and nanoarchitectures exhibited by the CoBi systems. Specifically, synthesis at an elevated growth temperature of 500 K resulted in CoBi nanowires. Reducing the growth temperature to 430 K led to the formation of rectangular CoBi islands via the Stranski–Krastanov mode. Further reduction to 100 K facilitated the coexistence of CoBi nanomeshs and large-scale CoBi islands. Conversely, growth at room temperature yielded a mix of CoBi and Co-doped Bi islands due to excess Bi. Moreover, STS revealed the presence of a Coulomb gap in either CoBi or Co-doped Bi islands. Our study not only demonstrates a novel cobalt pnictide system through MBE technology, but also provides an excellent platform for investigating the potential of high-temperature superconductivity and topological properties.

Declarations The authors declare that they have no competing interests and there are no conflicts.

Acknowledgements This work was supported by the National Natural Science Foundation of China (Nos. 12374196, 92165201, and 11634011), the Innovation Program for Quantum Science and Technology (No. 2021ZD0302800), the CAS Project for Young Scientists in Basic Research (Grant No. YSBR-046), the Fundamental Research Funds for the Central Universities (Grant Nos. WK3510000006 and WK3430000003), and Anhui Initiative in Quantum Information Technologies (No. AHY170000).

References

1. J. G. Bednorz and K. A. Müller, Possible high T_c superconductivity in the Ba–La–Cu–O system, *Z. Phys. B* 64(2), 189 (1986)
2. M. K. Wu, J. R. Ashburn, C. J. Torng, P. H. Hor, R. L. Meng, L. Gao, Z. J. Huang, Y. Q. Wang, and C. W. Chu, Superconductivity at 93 K in a new mixed-phase Yb–Ba–Cu–O compound system at ambient pressure, *Phys. Rev. Lett.* 58(9), 908 (1987)
3. A. Schilling, M. Cantoni, J. D. Guo, and H. R. Ott, Superconductivity above 130 K in the Hg–Ba–Ca–Cu–O system, *Nature* 363(6424), 56 (1993)
4. Y. Kamihara, T. Watanabe, M. Hirano, and H. Hosono, Iron-based layered superconductor $La[O_{1-x}F_x]FeAs$ ($x = 0.05$–0.12) with $T_c = 26$ K, *J. Am. Chem. Soc.* 130(11), 3296 (2008)
5. H. Takahashi, K. Igawa, K. Arii, Y. Kamihara, M. Hirano, and H. Hosono, Superconductivity at 43 K in an iron-based layered compound $LaO_{1-x}F_xFeAs$, *Nature* 453(7193), 376 (2008)
6. X. H. Chen, T. Wu, G. Wu, R. H. Liu, H. Chen, and D. F. Fang, Superconductivity at 43 K in $SmFeAsO_{1-x}F_x$, *Nature* 453(7196), 761 (2008)
7. D. X. Yao, Iron-based superconductors: A new family to find the origin of high T_c superconductivity, *Front. Phys.* 6(4), 344 (2011)
8. D. Li, K. Lee, B. Y. Wang, M. Osada, S. Crossley, H. R. Lee, Y. Cui, Y. Hikita, and H. Y. Hwang, Superconductivity in an infinite-layer nickelate, *Nature* 572(7771), 624 (2019)
9. M. Osada, B. Y. Wang, B. H. Goodge, S. P. Harvey, K. Lee, D. Li, L. F. Kourkoutis, and H. Y. Hwang, Nickelate superconductivity without rare-earth magnetism:$(La, Sr)NiO_2$, *Adv. Mater.* 33(45), 2104083 (2021)
10. S. Zeng, C. Li, L. E. Chow, Y. Cao, Z. Zhang, C. S. Tang, X. Yin, Z. S. Lim, J. Hu, P. Yang, and A. Ariando, Superconductivity in infinite-layer nickelate $La_{1-x}Ca_xNiO_2$ thin films, *Sci. Adv.* 8(7), eabl9927 (2022)
11. M. Xu, Y. Zhao, X. Ding, H. Leng, S. Zhang, J. Gong, H. Xiao, X. Zu, H. Luo, K. J. Zhou, B. Huang, and L. Qiao, Optimization for epitaxial fabrication of infinite-layer nickelate superconductors, *Front. Phys.* 19(3), 33209 (2024)
12. C. L. Song, Y. L. Wang, P. Cheng, Y. P. Jiang, W. Li, T. Zhang, Z. Li, K. He, L. Wang, J. F. Jia, H. H. Hung, C. Wu, X. Ma, X. Chen, and Q. K. Xue, Direct observation of nodes and two-fold symmetry in FeSe superconductor, *Science* 332(6036), 1410 (2011)
13. Q. Fan, W. H. Zhang, X. Liu, Y. J. Yan, M. Q. Ren, R. Peng, H. C. Xu, B. P. Xie, J. P. Hu, T. Zhang, and D. L. Feng, Plain s-wave superconductivity in single-layer FeSe on $SrTiO_3$ probed by scanning tunnelling microscopy, *Nat. Phys.* 11(11), 946 (2015)
14. C. Chen, Q. Liu, W. C. Bao, Y. Yan, Q. H. Wang, T. Zhang, and D. Feng, Observation of discrete conventional Caroli–de Gennes-Matricon states in the vortex core of single-layer $FeSe/SrTiO_3$, *Phys. Rev. Lett.* 124(9), 097001 (2020)
15. Q. Y. Wang, Z. Li, W. H. Zhang, Z. C. Zhang, J. S. Zhang, W. Li, H. Ding, Y. B. Ou, P. Deng, K. Chang, J. Wen, C. L. Song, K. He, J. F. Jia, S. H. Ji, Y. Y. Wang, L. L. Wang, X. Chen, X. C. Ma, and Q. K. Xue, Interface-induced high-temperature superconductivity in single unit-cell FeSe films $SrTiO_3$, *Chin. Phys. Lett.* 29(3), 037402 (2012)
16. S. He, J. He, W. Zhang, L. Zhao, D. Liu, X. Liu, D. Mou, Y. B. Ou, Q. Y. Wang, Z. Li, L. Wang, Y. Peng, Y. Liu, C. Chen, L. Yu, G. Liu, X. Dong, J. Zhang, C. Chen, Z. Xu, X. Chen, X. Ma, Q. Xue, and X. J. Zhou, Phase diagram and electronic indication of high-temperature superconductivity at 65 K in single-layer FeSe films, *Nat. Mater.* 12(7), 605 (2013)
17. B. Feng, J. Zhang, Q. Zhong, W. Li, S. Li, H. Li, P. Cheng, S. Meng, L. Chen, and K. Wu, Experimental realization of two-dimensional boron sheets, *Nat. Chem.* 8(6), 563 (2016)
18. J. L. Zhang, S. Zhao, C. Han, Z. Wang, S. Zhong, S. Sun, R. Guo, X. Zhou, C. D. Gu, K. D. Yuan, Z. Li, and W. Chen, Epitaxial growth of single layer blue

phosphorus: A new phase of two-dimensional phosphorus, *Nano Lett.* 16(8), 4903 (2016)
19. A. J. Mannix, Z. Zhang, N. P. Guisinger, B. I. Yakobson, and M. C. Hersam, Borophene as a prototype for synthetic 2D materials development, *Nat. Nanotechnol.* 13(6), 444 (2018)
20. M. Y. Huang, X. X. Jiang, Y. S. Zheng, Z. W. Xu, X. X. Xue, K. Q. Chen, and Y. X. Feng, Novel two-dimensional PdSe phase: A puckered material with excellent electronic and optical properties, *Front. Phys.* 17(5), 53504 (2022)
21. B. Lei, A. Li, W. Zhou, Y. Wang, W. Xiong, Y. Chen, and F. Ouyang, Room-temperature ferromagnetism and half-metallicity in monolayer orthorhombic CrS_2, *Front. Phys.* 19(4), 43200 (2024)
22. Z. Zhu, X. Cai, S. Yi, J. Chen, Y. Dai, C. Niu, Z. Guo, M. Xie, F. Liu, J. H. Cho, Y. Jia, and Z. Zhang, Multivalency-driven formation of Te-based monolayer materials: A combined first-principles and experimental study, *Phys. Rev. Lett.* 119(10), 106101 (2017)
23. Y. X. Wang, G. Qiu, R. X. Wang, S. Y. Huang, Q. X. Wang, Y. Y. Liu, Y. C. Du, W. A. III Goddard, M. J. Kim, X. F. Xu, P. D. Ye, and W. Z. Wu, Field-effect transistors made from solution-grown two-dimensional tellurene, *Nat. Electron.* 1(4), 228 (2018)
24. Z. J. Xie, C. Y. Xing, W. C. Huang, T. J. Fan, Z. J. Li, J. L. Zhao, Y. J. Xiang, Z. N. Guo, J. Q. Li, Z. G. Yang, B. Q. Dong, J. L. Qu, D. Y. Fan, and H. Zhang, Ultrathin 2D nonlayered tellurium nanosheets: Facile liquid-phase exfoliation, characterization, and photoresponse with high performance and enhanced stability, *Adv. Funct. Mater.* 28(16), 1705833 (2018)
25. W. Ding, J. Zeng, W. Qin, P. Cui, and Z. Zhang, Exploring high transition temperature superconductivity in a freestanding or $SrTiO_3$-supported CoSb monolayer, *Phys. Rev. Lett.* 124(2), 027002 (2020)
26. J. Gao, W. Ding, S. Zhang, Z. Zhang, and P. Cui, Coexistence of superconductivity and nontrivial band topology in monolayered cobalt pnictides on $SrTiO_3$, *Nano Lett.* 21(17), 7396 (2021)
27. C. Ding, G. Gong, Y. Liu, F. Zheng, Z. Zhang, H. Yang, Z. Li, Y. Xing, J. Ge, K. He, W. Li, P. Zhang, J. Wang, L. Wang, and Q. K. Xue, Signature of superconductivity in orthorhombic CoSb monolayer films on $SrTiO_3$, *ACS Nano* 13(9), 10434 (2019)
28. R. Lou, M. Y. A. Lei, W. J. Ding, W. T. Yang, X. Y. Chen, R. Tao, S. Y. Ding, X. P. Shen, Y. J. Yan, P. Cui, H. C. Xu, R. Peng, T. Zhang, Z. Y. Zhang, and D. L. Feng, Electronic structure and signature of Tomonaga–Luttinger liquid state in epitaxial $CoSb_{1-x}$ nanoribbons, *npj Quantum Mater.* 6(1), 79 (2021)
29. J. J. Lee, F. T. Schmitt, R. G. Moore, S. Johnston, Y. T. Cui, W. Li, M. Yi, Z. K. Liu, M. Hashimoto, Y. Zhang, D. H. Lu, T. P. Devereaux, D. H. Lee, and Z. X. Shen, Interfacial mode coupling as the origin of the enhancement of T_c in FeSe films on $SrTiO_3$, *Nature* 515(7526), 245 (2014)
30. S. Gerber, S. L. Yang, D. Zhu, H. Soifer, J. A. Sobota, S. Rebec, J. J. Lee, T. Jia, B. Moritz, C. Jia, A. Gauthier, Y. Li, D. Leuenberger, Y. Zhang, L. Chaix, W. Li, H. Jang, J. S. Lee, M. Yi, G. L. Dakovski, S. Song, J. M. Glownia, S. Nelson, K. W. Kim, Y. D. Chuang, Z. Hussain, R. G. Moore, T. P. Devereaux, W. S. Lee, P. S. Kirchmann, and Z. X. Shen, Femtosecond electron–phonon lock-in by photoemission and X-ray free-electron laser, *Science* 357(6346), 71 (2017)
31. S. Zhang, T. Wei, J. Guan, Q. Zhu, W. Qin, W. Wang, J. Zhang, E. W. Plummer, X. Zhu, Z. Zhang, and J. Guo, Enhanced superconducting state in $FeSe/SrTiO_3$ by a dynamic interfacial polaron mechanism, *Phys. Rev. Lett.* 122(6), 066802 (2019)
32. I. Horcas, R. Fernandez, J. M. Gomez-Rodriguez, J. Colchero, J. Gomez-Herrero, and A. M. Baro, WSXM: A software for scanning probe microscopy and a tool for nanotechnology, *Rev. Sci. Instrum.* 78(1), 013705 (2007)
33. S. Qin, J. Kim, Q. Niu, and C. K. Shih, Superconductivity at the two-dimensional limit, *Science* 324(5932), 1314 (2009)
34. F. Cai, P. Li, K. Xie, R. Tang, and S. Qin, Superconductivity of Pb films studied with superconducting Pb tips, *Sci. China Phys. Mech.* 62(1), 1 (2018)
35. R. Feng, E. H. Conrad, M. C. Tringides, C. Kim, and P. F. Miceli, Wetting-layer transformation for Pb nanocrystals grown on Si(111), *Appl. Phys. Lett.* 85(17), 3866 (2004)
36. R. M. Tromp, R. J. Hamers, and J. E. Demuth, Si(001) dimer structure observed with scanning tunneling microscopy, *Phys. Rev. Lett.* 55(12), 1303 (1985)
37. W. Zhou, X. Zou, S. Najmaei, Z. Liu, Y. Shi, J. Kong, J. Lou, P. M. Ajayan, B. I. Yakobson, and J. C. Idrobo, Intrinsic structural defects in monolayer molybdenum disulfide, *Nano Lett.* 13(6), 2615 (2013)
38. G. Springholz and K. Wiesauer, Nanoscale dislocation patterning in PbTe/PbSe(001) lattice-mismatched heteroepitaxy, *Phys. Rev. Lett.* 88(1), 015507 (2001)
39. L. Sudheendra, V. Moshnyaga, E. D. Mishina, B. Damaschke, T. Rasing, and K. Samwer, Direct imaging of lattice-strain-induced stripe phases in an optimally doped manganite film, *Phys. Rev. B* 75(17), 172407 (2007)
40. J. Wright, C. Chang, D. Waters, F. Lupke, R. Feenstra, L. Raymond, R. Koscica, G. Khalsa, D. Muller, H. G. Xing, and D. Jena, Unexplored MBE growth mode reveals new properties of superconducting NbN, *Phys. Rev. Mater.* 5(2), 024802 (2021)
41. A. Rajan, K. Underwood, F. Mazzola, and P. D. C. King, Morphology control of epitaxial monolayer transition metal dichalcogenides, *Phys. Rev. Mater.* 4(1), 014003 (2020)
42. Y. H. Yuan, X. T. Wang, C. L. Song, L. L. Wang, K. He, X. C. Ma, H. Yao, W. Li, and Q. K. Xue, Observation of coulomb gap and enhanced superconducting gap in nano-sized Pb islands grown on $SrTiO_3$, *Chin. Phys. Lett.* 37(1), 017402 (2020)